catalysts

MDPI

Article

Acid–Base Bifunctional Hf Nanohybrids Enable High Selectivity in the Catalytic Conversion of Ethyl Levulinate to γ-Valerolactone

Weibo Wu, Yan Li, Hu Li *, Wenfeng Zhao and Song Yang *

State Key Laboratory Breeding Base of Green Pesticide & Agricultural Bioengineering, Key Laboratory of Green Pesticide & Agricultural Bioengineering, Ministry of Education, State-Local Joint Laboratory for Comprehensive Utilization of Biomass, Center for Research & Development of Fine Chemicals, Guizhou University, Guiyang, Guizhou 550025, China; weibo_wu666@126.com (W.W.); ly15761698544@163.com (Y.L.); zwf2018gudx@126.com (W.Z.)

* Correspondence: hli13@gzu.edu.cn (H.L.); jhzx.msm@gmail.com (S.Y.); Tel.: +86-183-0261-4827 (H.L.); +86-851-8829-2171 (S.Y.)

Received: 26 May 2018; Accepted: 26 June 2018; Published: 29 June 2018

Abstract: The catalytic upgrading of bio-based platform molecules is a promising approach for biomass valorization. However, most solid catalysts are not thermally or chemically stable, and are difficult to prepare. In this study, a stable organic phosphonate–hafnium solid catalyst (PPOA–Hf) was synthesized, and acid–base bifunctional sites were found to play a cooperative role in the cascade transfer hydrogenation and cyclization of ethyl levulinate (EL) to γ-valerolactone (GVL). Under relatively mild reaction conditions of 160 °C for 6 h, EL was completely converted to GVL with a good yield of 85%. The apparent activation energy was calculated to be 53 kJ/mol, which was lower than other solid catalysts for the same reaction. In addition, the PPOA-Hf solid catalyst did not significantly decrease its activity after five recycles, and no evident leaching of Hf was observed, indicating its high stability and potential practical application.

Keywords: heterogeneous catalysis; transfer hydrogenation; biomass conversion; biofuels; catalytic materials

1. Introduction

Nowadays, with the continuous development of human society, the demand for energy and fine chemicals is increasing [1]. However, the use and gradual depletion of fossil resources need people to face and solve a series of problems, such as environmental pollution, greenhouse effects, and the energy crisis [2]. The development of renewable energy is, thus, highly demanded, where biomass sources are the only sustainable organic carbon feedstock, showing great potential for practical applications [3]. Lignocellulose is abundant in nature and was demonstrated as capable of being efficiently converted to a series of highly valuable chemicals and biofuels through chemo-catalytic reactions coupled with well-designed processes [4,5].

As a biomass-derived versatile platform molecule, γ-valerolactone (GVL) can be used as a green solvent for biomass conversion and organic transformations [6]. In addition, it can be employed for producing biofuels and fuel additives (e.g., 2-methyltetrahydrofuran) [7], and as a key intermediate in the synthesis of fine chemicals (e.g., pentenoic acid and α-methylene-γ-valerolactone (MeGVL)), as shown in Scheme 1 [8,9]. Typically, GVL can be prepared from lignocellulose via sequential catalytic pathways involving various reactions such as hydrolysis, isomerization, dehydration, etherification, esterification, hydrogenation, and lactonization [10–16]. Amongst these conversion processes, cascade hydrogenation and cyclization were deemed in recent years as the key step in catalytically upgrading levulinic acid and its esters to GVL [17,18].

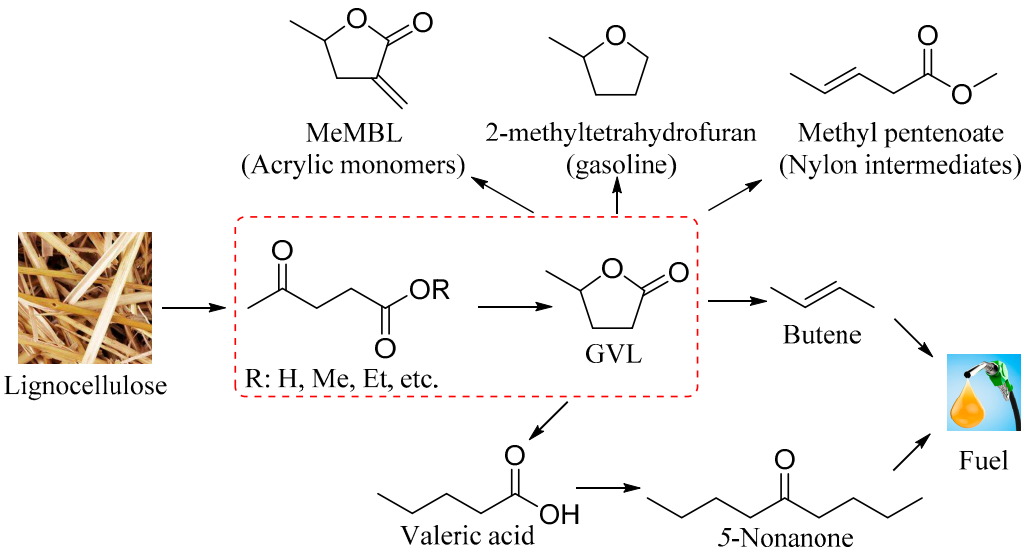

Scheme 1. Synthesis and application of γ-valerolactone (GVL).

Catalytic transfer hydrogenation (CTH) is widely used in the reduction of carbonyl compounds, where H_2 gas is replaced by other liquid molecules (e.g., formic acid and alcohols) as hydrogen donors [19–21]. It is worth noting that there is a certain requirement for the quality of the used reactor and the catalyst stability to tolerate acidic reaction conditions [22,23]. In this regard, alcohols seem to be a better candidate for CTH. A well-known example, Zr-incorporated zeolites with appropriate Lewis acidity, were reported as able to efficiently catalyze the CTH of biomass-derived carboxides, alike to the Meerwein–Ponndorf–Verley (MPV) reduction [24–26].

In the past decade, Zr-based catalysts were reported as efficient for the CTH of levulinic acid and its esters to GVL, and their reactivity is highly dependent on the catalyst composition. For instance, ZrO_2 [27,28], $Zr(OH)_4$ [29], $ZrFeO_x$ [30], Al–Zr [31], Zr–B [32], and $ZrOCl_2$ [33] need relatively harsh conditions (ca. 200 °C or >6 h) to achieve moderate yields of GVL (Table 1). The stability and catalytic performance can be improved via the incorporation of Zr species into solid supports like SBA-15 (Santa Barbara Amorphous-15); however, it generally involves complicated preparation procedures and relatively high production costs due to the use of expensive template agents [34]. Therefore, it is necessary to overcome these shortcomings by improving the stability of solid catalysts with a facile preparation method.

Table 1. Activity contrast of previous studies in the conversion of ethyl levulinate (EL) into γ-valerolactone (GVL).

Entry	Catalyst	Temp (°C)	Time (h)	GVL Yield (%)	EL Conversion (%)	Reference
1	ZrO_2	180	4	80	93	[27]
2	ZrO_2	250	1	63	82	[28]
3	$Zr(OH)_4$	240	3	80	99	[29]
4	ZrFeO(1:3)-300	230	3	87	93	[30]
5	Al_7Zr_3-300	220	4	83	96	[31]
6	Zr_1B_1	200	4	88	95	[32]
7	PPOA–Hf-1:1.5	160	6	85	100	This work

Organic phosphonates as ligands combined with metal ions can react quickly under liquid-phase conditions to afford corresponding inorganic–organic metal phosphonates with enhanced chemical and thermal stability [35–41]. Through the coordination of metal ions with organic phosphoric acid, additional micro- and mesopores are introduced into the resulting catalysts, thus greatly increasing specific surface areas [42,43], and the catalyst functionalities can be simply tuned by changing the organic ligand or preparation method [44]. In the presented study, a novel and stable inorganic–organic

metal phosphonate catalyst (PPOA–Hf) was prepared from phenylphosphonic acid (PPOA) and hafnium (Hf, in the same group as Zr on the periodic table) chloride using a simple assembly method. This acid–base bifunctional solid catalyst was able to efficiently promote the conversion of EL into GVL under mild reaction conditions, and systematic studies were thereby conducted.

2. Results and Discussions

2.1. Catalyst Characterization

Prior to conducting catalytic reactions, HfO_2 and PPOA–Hf-1:1.5 were characterized using Brunauer–Emmett–Teller (BET), scanning transmission electron microscopy (STEM), transmission electron microscopy (TEM), thermogravimetry (TG), X-ray diffraction (XRD), and pyridine-absorbed infrared (PY-IR) spectroscopy. Compared to HfO_2 having a low surface area (23 m^2/g) with a large average pore diameter (28.9 nm), PPOA–Hf-1:1.5 was examined to be mesoporous (average pore diameter: 3.4 nm) with a surface area of 215 m^2/g and a pore volume of 0.16 cm^3/g using N_2 adsorption–desorption isotherms (Figures 1A and S1). From the PY-IR spectra in Figure 1B, a characteristic peak can be seen at 1450 cm^{-1}, which is indicative of Lewis acid sites in PPOA–Hf-1:1.5. Moreover, there were small peaks at 1490 cm^{-1} and 1520 cm^{-1}, showing the presence of weak Brønsted acid sites in PPOA–Hf-1:1.5. In contrast, HfO_2 lacks Brønsted acid sites. The hydrogen transfer reaction is typically catalyzed by Lewis acid sites, while Brønsted acid sites present in PPOA–Hf-1:1.5 may promote the adsorption of substrates, as well as the lactonization step. TG analysis was conducted to study the thermal stability of PPOA–Hf and HfO_2 (Figure 1C). It is interesting to note that less than 10% of the catalyst weight was lost until 400 °C, beyond which PPOA–Hf showed better stability than HfO_2. Increased weight loss was observed upon reaching 550 °C. This result indicates that the PPOA–Hf catalyst is thermally stable, and can be a good candidate for chemical reactions under thermal conditions. XRD analyses show that the commercial catalyst, HfO_2, has a good crystalline form (JPCDS # 06-0318), while PPOA–Hf does not have a highly crystalline nature (Figure 1D), with some broad bands belonging to tetragonal (t) and monoclinic (m) phases. Furthermore, the peak at $2\theta = 6°$ possibly resulted from the interlayer clearance of the phosphate [45].

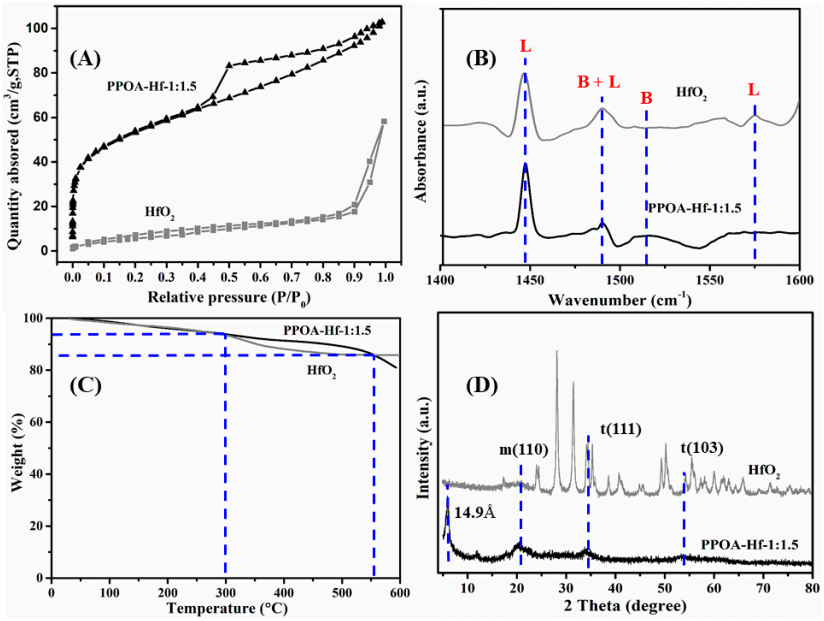

Figure 1. N_2 adsorption–desorption isotherms (**A**); pyridine-adsorbed infrared (IR) spectra (**B**); thermogravimetry (TG) curves (**C**); and X-ray diffraction (XRD) patterns (**D**) of HfO_2 and the phosphonate–hafnium solid catalyst (PPOA–Hf-1:1.5); L = Lewis acid; B = Brønsted acid.

TEM images further confirmed that PPOA–Hf-1:1.5 (Figure 2A) is non-crystalline when compared with HfO_2 (Figure 2B), and the detected lamellar structure is consistent with the result ($2\theta = 6^\circ$) clarified using XRD (Figure 1A). Gratifyingly, the particle size of PPOA–Hf-1:1.5 seems to be smaller than that of HfO_2 (Figure 2), due to its amorphous structure. Furthermore, STEM elemental mappings indicate the even and well-connected combination of the organic ligand and Hf (Figure S2).

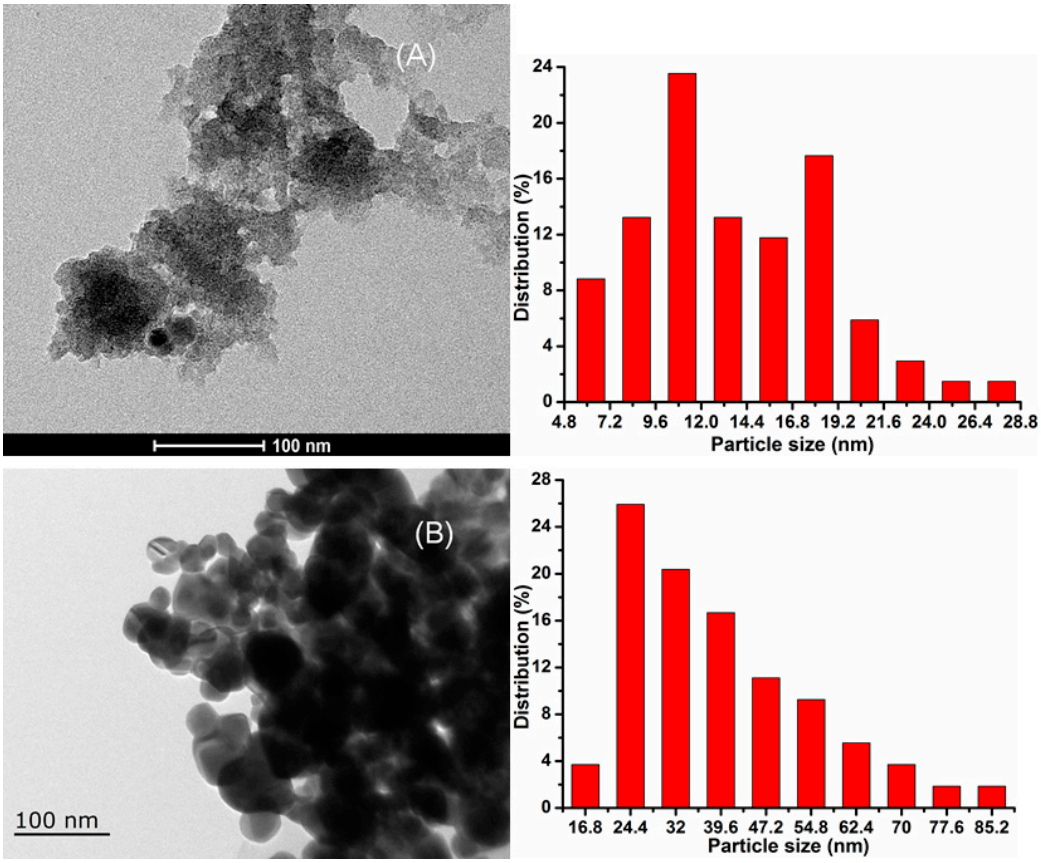

Figure 2. Transmission electron microscopy (TEM) images and particle size distribution of (**A**) PPOA–Hf-1:1.5, and (**B**) HfO_2.

The base and acid properties of the PPOA–Hf-*x* catalysts in various molar ratios of PPOA/Hf were determined using CO_2-temperature programmed desorption (TPD) and NH_3-TPD, respectively. As shown in Figure 3, it can be clearly observed that PPOA–Hf is an acid–base bifunctional catalyst, and the contents of the acid and base sites increase with the increase in Hf relative to PPOA. The Lewis acid and base sites were Hf^{4+} and O^{2-} species, respectively, and their contents increased with the augmentation of Hf, due to the appropriate formation of Hf–O–P. Notably, the acid–base site density remained nearly unchanged after recycling five times (Table S1), indicating that the PPOA–Hf catalyst was stable and reusable.

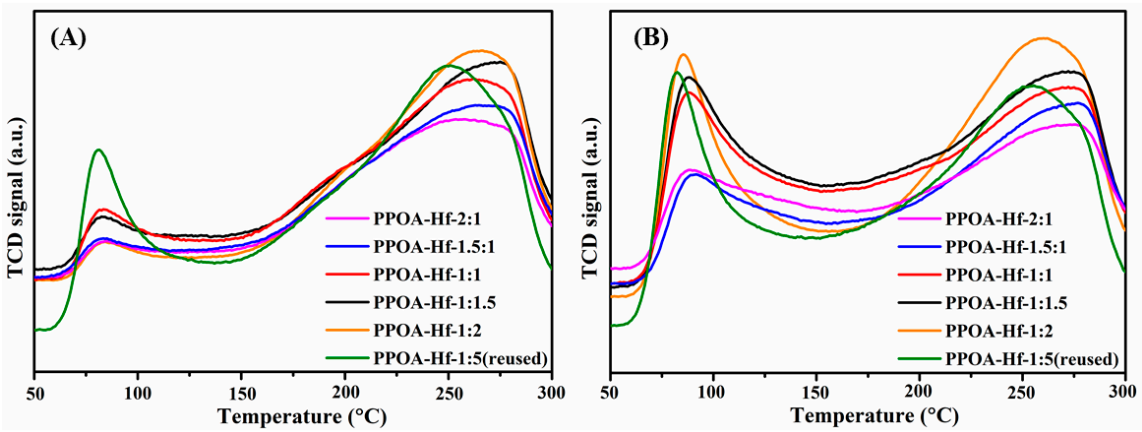

Figure 3. CO_2- temperature programmed desorption (TPD) (**A**), and NH_3-TPD (**B**) patterns of PPOA–Hf-*x* with various PPOA/Hf molar ratios.

The strengths of the acid and base sites were investigated using X-ray photoelectron spectroscopy (XPS) analysis, and the results are provided in Figures 4 and S3, and Table S2. Typically, low and high binding energy of O 1s and Hf 4f are indicative of the high strength of both base and acid sites [46]. The binding energy intensity of Hf 4f (Lewis acid) in PPOA–Hf shows the positive charge on the Hf atoms, which resulted in a stronger Lewis acidity with a higher Hf ratio [47]. Furthermore, the binding energy of the O element was also studied, where the lower binding energy of O 1s was correlated with a higher negative charge on the O atom, which resulted in stronger Lewis basicity of O [48]. It is not difficult to see that the strength of acidic and basic sites in the PPOA–Hf-*x* catalysts is negatively correlated with the increase in PPOA/Hf ratio (Figure 4). In this respect, both the content and strength of acid–base sites in PPOA–Hf-*x* can be controlled by adjusting the molar ratio of PPOA/Hf.

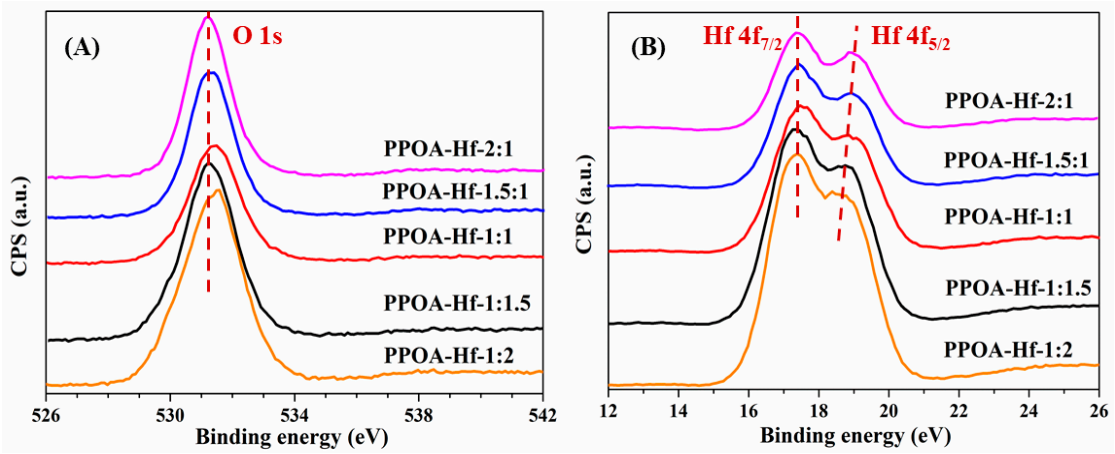

Figure 4. X-ray photoelectron spectroscopy (XPS) spectra of (**A**) O 1s, and (**B**) Hf 4f in PPOA–Hf-*x* with various PPOA/Hf molar ratios.

To clearly elucidate the functional structure of PPOA–Hf-*x*, Fourier-transform infrared (FT-IR) spectroscopy was conducted, and the spectra are shown in Figure 5. In area A, the peak of Hf–O (500–800 cm^{-1}) is clearly visible in the spark line of HfO_2. On the other hand, the peaks at 600 cm^{-1} (corresponding to an aromatic ring) and 700 cm^{-1} (out-of-plane bending vibration of a C–H bond) decreased sharply with an increase in Hf content, implying the tight combination of hafnium and the organic ligand. Interestingly, with the combination of PPOA and Hf, the positions of the O–H (2400–3200 cm^{-1}) bond and the Ph–H (1900–2300 cm^{-1}) bond shifted to 3200–3700 cm^{-1} and

3000–3100 cm^{-1}, respectively. In addition, the characteristic peaks of the P–O (1000 cm^{-1}), C–P (1150–1200 cm^{-1}), and C=C (1400–1700 cm^{-1}) bonds were all present, indicating the strong connection between the organic ligand and Hf, and the possible origin of acid and base sites (e.g., Brønsted acid sites: −OH; Lewis acid-base sites: –Hf–O–P–).

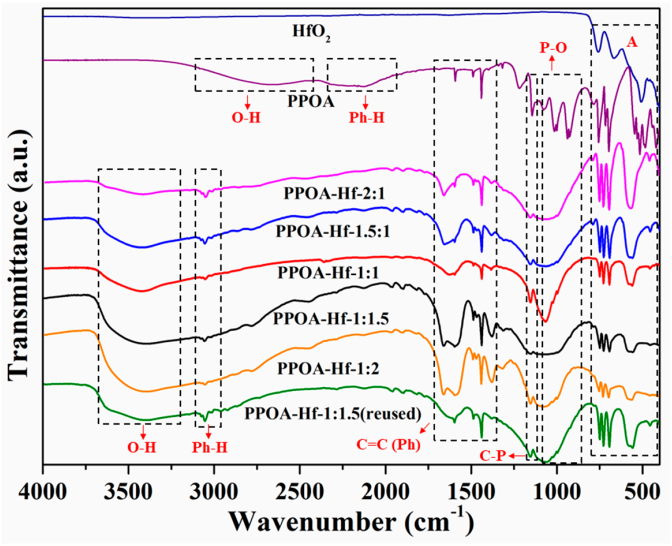

Figure 5. Fourier-transform infrared (FT-IR) spectra of PPOA–Hf–*x* with various PPOA/Hf molar ratios.

2.2. Catalytic Performance of PPOA–Hf-x

The catalytic activity of PPOA–Hf-x with various PPOA/Hf molar ratios in the CTH reaction of EL to GVL was investigated at first, and the results are shown in Figure 6. It is obvious that as the ratio of PPOA/Hf changed from 2:1 to 1:1.5, the conversion rate of EL and the yield of GVL increased from 72% and 55% to 100% and 85%, respectively. This tendency is approximately consistent with the content and strength of the acid–base sites (Figures 3 and 4B). However, a further increase in the PPOA/Hf ratio to 1:2 did not improve the yield of GVL, showing that the acidity and basicity of PPOA–Hf-1:1.5 is appropriate for GVL synthesis from EL. Therefore, PPOA–Hf-1:1.5 was considered as the optimal catalyst for subsequent studies.

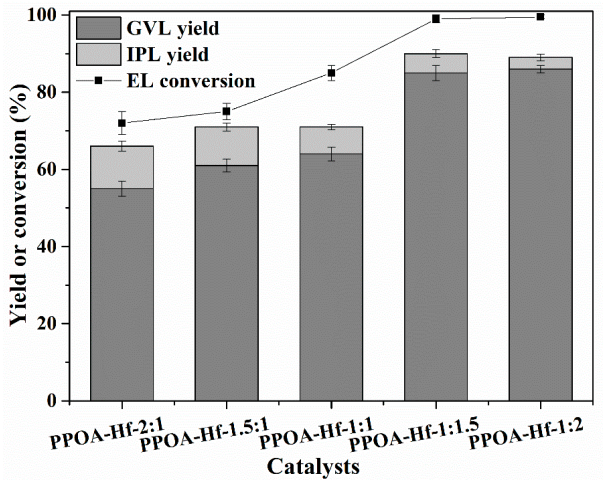

Figure 6. Catalytic results of PPOA–Hf-*x* with various PPOA/Hf molar ratios in the conversion of ethyl levulinate (EL) to GVL. Reaction conditions: EL, 1 mmol; catalyst, 72 mg; 2-propanol, 5 mL; T, 160 °C; and *t*, 6 h.

In the study of the mechanism, the acid–base sites in PPOA–Hf-1:1.5 played a cooperative role in the reaction of EL to GVL (Scheme 2). Firstly, 2-propanol was activated via combination with the Lewis acid sites (Hf^{4+}) and Lewis base sites (O^{2-}) of PPOA–Hf. Concurrently, the carbonyl group in EL was activated via the Lewis acid sites (Hf^{4+}). As a result, a hydrogen transfer reaction was carried out successfully with PPOA–Hf-1:1.5. Subsequently, lactonization occurred via a five-membered ring, which was facilitated by the Brønsted acid. Notably, more than 90% carbon balance was detected for the conversion of EL to GVL.

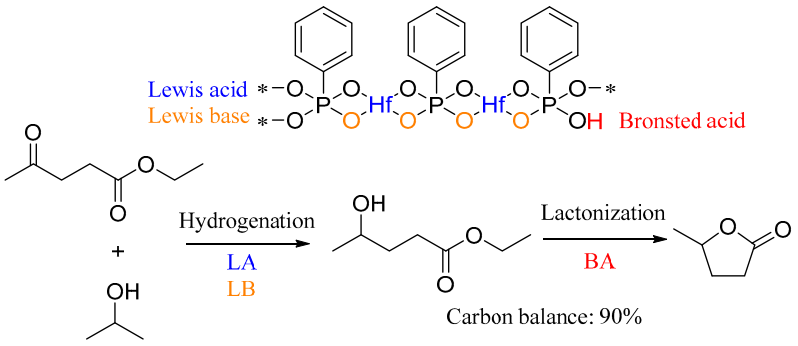

Scheme 2. Reaction pathways for the conversion of ethyl levulinate (EL) to GVL, catalyzed by the phosphonate–hafnium solid catalyst (PPOA–Hf-1:1.5); LA = Lewis acid; LB = Lewis base; BA = Brønsted acid.

2.3. *Effect of Reaction Time and Temperature*

Reaction temperature and time are important parameters for reactivity control in chemical reactions. The effect of reaction temperature (120–180 °C) on the conversion of EL to GVL catalyzed by PPOA–Hf-1:1.5 over 6 h was studied, and the results are shown in Figure 7. Relatively high yield of GVL (ca. 85%) was obtained in 6 h at 160 °C, and in 4 h at 180 °C. Isopropyl levulinate (IPL) was detected as the dominant byproduct, which reduced the selectivity of GVL. From an economic point of view, the optimal reaction conditions should be 160 °C and 6 h.

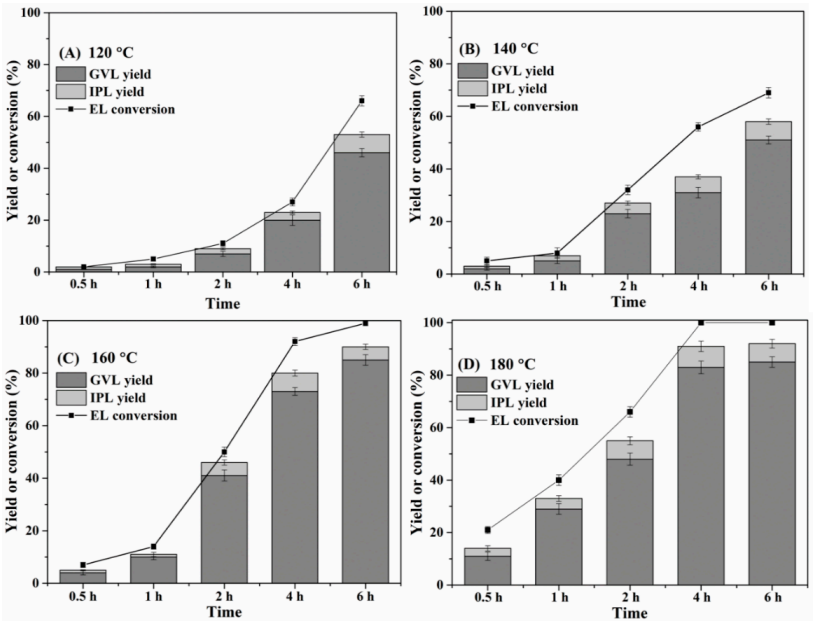

Figure 7. Effect of reaction temperature (120–180 °C) and time on the conversion of EL to GVL. Reaction conditions: EL, 1 mmol; PPOA–Hf-1:1.5, 72 mg; and 2-propanol, 5 mL.

The kinetics of the EL-to-GVL conversion were studied under the assumption of a pseudo first-order reaction, as illustrated in previous reports [49]. In this study, four reaction temperatures of 120 °C (393 K), 140 °C (413 K), 160 °C (433 K), and 180 °C (453 K) were selected. Well-fitted linear curves were obtained by plotting $-\ln(1-X)$ (X = EL conversion) with time for various reaction temperatures, as shown in Figure 8A. The apparent activation energy (E_a) was calculated to be 53 kJ/mol according to the Arrhenius equation, after the obtained reaction rate constant ($\ln k$) was plotted with temperature (1/T; Figure 8B). This value is much lower than other previously reported catalytic systems, such as Ti-Beta (69 kJ/mol) [49], Shvo-Ru (69 kJ/mol) [50], and Ru tris(m-sulfonatophenyl)phosphine (61 kJ/mol) [51], indicating that PPOA–Hf-1:1.5 is a more effective and promising solid catalyst for the catalytic conversion of EL to GVL.

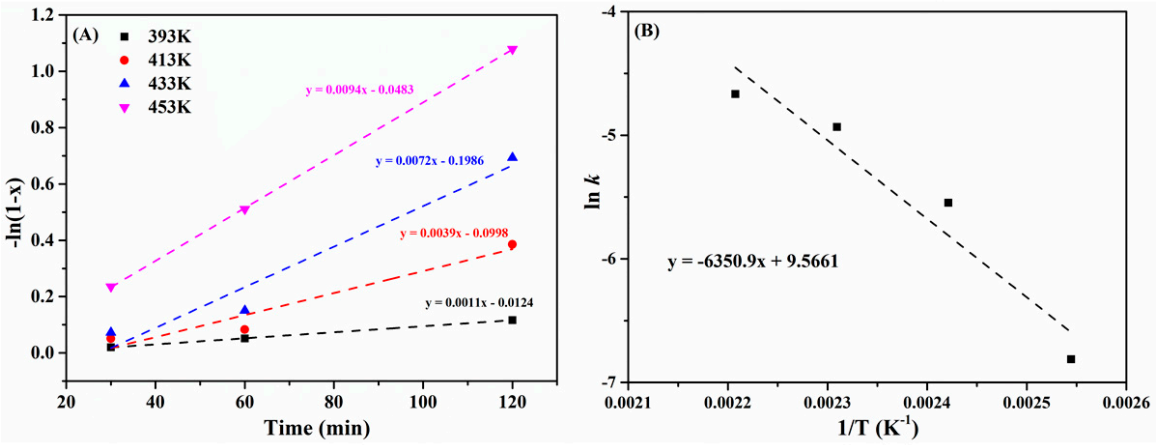

Figure 8. (**A**) Kinetic profiles, and (**B**) Arrhenius plot of the PPOA–Hf-1:1.5-catalyzed conversion of EL to GVL. Reaction conditions: EL, 1 mmol; PPOA–Hf-1:1.5, 72 mg; and 2-propanol, 5 mL.

2.4. Effect of Catalyst Dosage and Reactivity Comparison with Various Catalysts

In this section, the influence of catalyst dosage was examined (Figure 9). The absence of catalyst led to almost no GVL formed, indicating that the reaction required the participation of the catalyst. When the catalyst dosage increased, the yield of GVL rose accordingly. At a catalyst dosage of 72 mg, both the GVL yield and EL conversion reached a maximum. There was no further increase in GVL yield when more than 72 mg PPOA–Hf-1:1.5 was used, indicating that 72 mg (mass ratio 2:1) is the best catalyst dosage.

For comparison, several oxides and the precursor, PPOA, were used for the catalytic conversion of EL to GVL (Table 2). Weak acids or base oxides, such as SiO_2, TiO_2, and MgO, had nearly no catalytic activity for the reaction. In contrast, amphoteric oxides, including HfO_2, Al_2O_3, and ZrO_2, produced GVL in low yields of 6%, 1%, and 2%, respectively. PPOA, due to its high acidity, could catalyze the conversion of EL into IPL (13% yield). Notably, when a strong base (CaO) was used, a 17% yield of GVL and a 43% yield of IPL were obtained. Considering the above results, it can be deduced that base sites are helpful for GVL synthesis, while potentially resulting in the formation of IPL. On the other hand, strong acids in the absence of Lewis acid species are unable to catalyze the production of GVL, while potentially promoting the cyclization or lactonization steps. Due to the appropriate acid–base site content and strength, PPOA–Hf-1:1.5 can efficiently catalyze the synthesis of GVL (85% yield) from EL, with a yield much higher than other tested catalysts. Moreover, hafnium has stronger metal properties than zirconium. Accordingly, there is a weaker Lewis acid in the Zr-based organic phosphonic acid ligand catalyst (PPOA–Zr-1:1.5), which, when produced using the same method as PPOA–Hf-1:1.5, resulted in PPOA–Zr-1:1.5 showing a relatively poor catalytic performance (Table 2, entry 10).

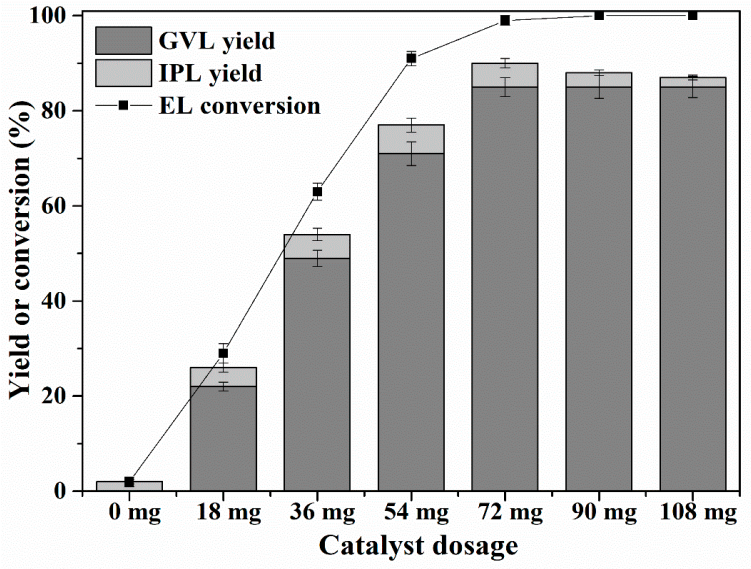

Figure 9. Effect of catalyst dosage on the conversion of EL to GVL. Reaction conditions: EL, 1 mmol; 2-propanol, 5 mL; T, 160 °C; and *t*, 6 h.

Table 2. Activity comparison of various solid catalysts in the conversion of EL to GVL [a].

Entry	Catalyst	GVL Yield (%)	IPL Yield (%)	EL Conversion (%)	Average Rate (μmol $g^{-1}h^{-1}$) [b]
1	SiO_2	<1	<1	1	<20
2	TiO_2	<1	<1	1	<20
3	MgO	<1	<1	1	<20
4	HfO_2	6	1	10	140
5	Al_2O_3	1	5	8	23
6	ZrO_2	2	-	5	46
7	PPOA	0	13	16	-
8	CaO	17	43	81	400
9	PPOA–Hf-1:1.5	85	5	100	1970
10	PPOA–Zr-1:1.5	73	6	90	1690

[a] Reaction conditions: EL, 1 mmol; catalyst, 72 mg; 2-propanol, 5 mL; T, 160 °C; and *t*, 6 h. [b] Average rate is defined as (mol of formed GVL)/(catalyst weight × time).

2.5. Catalyst Leaching Experiments and Recycling Study

Based on the results of the TG analysis, the catalyst has good thermal stability. To examine the chemical stability of the solid catalyst (PPOA–Hf-1:1.5), a hot filtration experiment was carried out. During the catalytic conversion of EL to GVL, PPOA–Hf-1:1.5 was filtered out after 3 h as soon as the reaction system cooled to ca. 80 °C. Then, the GVL yield was measured per hour for the next three hours. No significant increase in GVL yield was observed (Figure 10), and ICP analysis shows that almost no Hf and P were leached (<0.01 ppm). This result demonstrates that PPOA–Hf-1:1.5 is a heterogeneous catalyst, and is chemically stable in the reaction system.

Furthermore, the reusability of the solid catalyst was investigated (Figure 11), and the PPOA–Hf catalyst could be reused five consecutive times without a significant reduction in GVL yield and EL conversion. The IR spectra in Figure 7 show that the reused catalyst kept an intact structure after being recycled five times. In addition, the acid and base activity sites were retained in the reused catalyst, as illustrated by the NH_3-TPD and CO_2-TPD (Figure 4). These results prove the good reusability of the solid catalyst, PPOA–Hf.

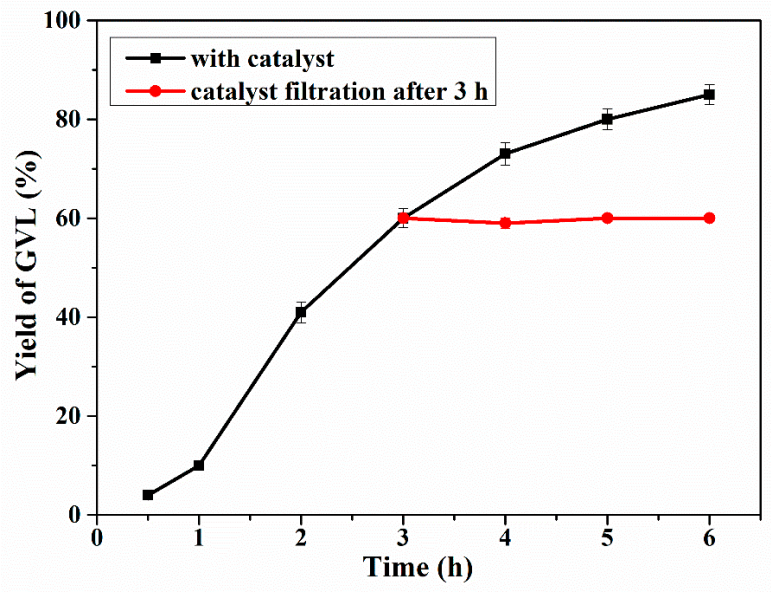

Figure 10. Hot filtration experimental results of the PPOA–Hf-1:1.5-catalyzed conversion of EL to GVL. Reaction conditions: EL, 1 mmol; PPOA–Hf-1:1.5, 72 mg; 2-propanol, 5 mL; and T, 160 °C.

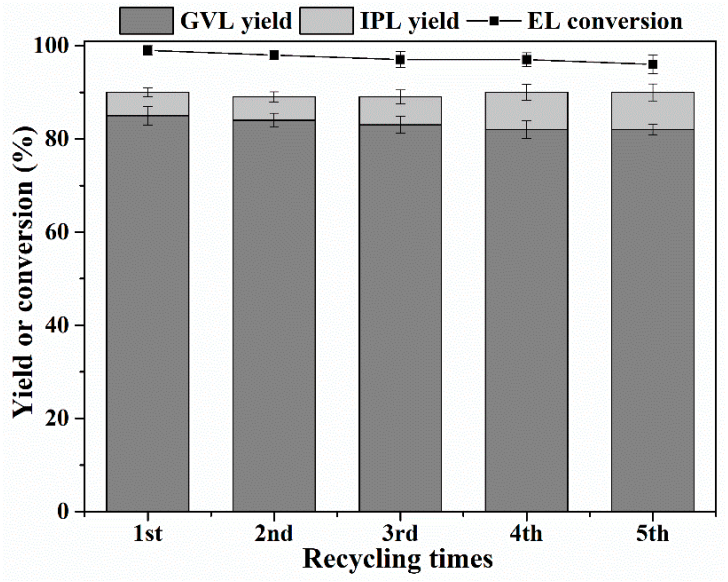

Figure 11. Reusability of PPOA–Hf-1:1.5 in the catalytic conversion of EL to GVL. Reaction conditions: EL, 1 mmol; PPOA–Hf-1:1.5, 72 mg; 2-propanol, 5 mL; T, 160 °C; and *t*, 6 h.

3. Materials and Experiments

3.1. Materials

Hafnium (IV) chloride ($HfCl_4$; 99%), hafnium (IV) oxide, and phenylphosphonic acid (PPOA, 98%) were purchased from Adamas Reagent Co., Ltd. (Shanghai, China) Ethyl levulinate (EL; 98%) was purchased from Alfa Aesar (Shanghai, China) Chemicals Co., Ltd. Naphthalene (99%), γ-valerolactone (GVL; 98%), 2-propanol (99.5%), and other reagents were purchased from Beijing Innochem Technology Co., Ltd. (Beijing, China), and were directly used for the study unless otherwise noted.

3.2. Catalyst Preparation

Hafnium phenylphosphonates (PPOA–Hf-*x*; *x* denotes the used molar ratio of PPOA to Hf) were prepared from PPOA and $HfCl_4$ with corresponding PPOA/Hf ratios. In a typical procedure for the synthesis of PPOA–Hf-1:1.5, 20 mmol PPOA (0.3162 g) was initially dissolved into 60 mL of *N*,*N*-dimethylformamide (DMF) in a Teflon-lined tube, followed by a dropwise addition of 30 mmol $HfCl_4$ (0.9609 g) under vigorous stirring conditions. After stirring for 20 min, the hydrothermal reactor was sealed and placed into an oven heated to 120 °C, for 24 h. Upon completion, the solid precipitates were separated from the liquid mixture via filtration, then successively washed with DMF (100 mL), ethanol (100 mL), and methanol (100 mL) 2–3 times, and finally, dried at 45 °C overnight to give the catalyst, PPOA–Hf-1:1.5.

3.3. Catalyst Characterization Techniques

Brunauer–Emmett–Teller (BET) surface areas of the porous materials were determined from nitrogen physisorption measurements at liquid-nitrogen temperature on a Micromeritics ASAP 2460 instrument (Micromeritics, Norcross, GA, USA). Fourier-transform infrared (FT-IR) spectra were measured by a Thermo Fisher Nicolet iS50 spectrometer (Thermo Fisher Scientific, Waltham, MA, USA) with a wavenumber range of 400–4000 cm^{-1}. The Lewis and Brønsted acid sites of PPOA–Hf were determined via a vacuum adsorption surface reaction infrared in situ characterization analysis system (Dalian Institute of Chemical Physics, Chinese Academy of Sciences, Dalian, China) with a Thermo Fisher Nicolet iS50 AEM with a wavenumber range of 1400–1600 cm^{-1}. Contents of Hf and P species in the reaction system were determined using an inductively coupled plasma-optical emission spectrometer (ICP-OES) on a PerkinElmer Optima 5300 DV (LabX, Midland, Canada). Scanning transmission electron microscopy (STEM) and transmission electron microscopy (TEM) tests were measured using a JEOL 2100 TEM/STEM (JEOL, Akishima, Japan). Particle size distribution was calculated via the Nano Measurer 1.2, Visual Basic 6.0 software. Thermogravimetry (TG) analysis was carried out using a NETZSCH STA 449 F3 Jupiter thermal gravimetric analyzer (NETZSCH, Selb, German). The acidity and basicity of the catalysts were measured by NH_3-temperature programmed desorption (TPD) and CO_2-TPD using a Micromeritics AutoChem 2920 chemisorption analyzer (Micromeritics, Norcross, GA, USA). The pyridine adsorption process was carried out at room temperature, followed by heating to 100 °C, and kept for 5 min. Then, the spectrum was obtained after cooling down to room temperature. X-ray photoelectron spectroscopy (XPS) measurements were recorded using a Physical Electronics Quantum 2000 Scanning ESCA Microprobe (Physical Electronics Inc., Chanhassen, MN, USA) equipped with a monochromatic Al Kα anode. The X-ray diffraction (XRD) (Rigaku, Akishima, Japan) data of the powder samples were obtained using a Rigaku International D/max-TTR III X-ray powder diffractometer with Cu Kα radiation, and 2θ scanned from 5° to 80°.

3.4. Catalytic Activity Measurements

The reactions for the conversion of EL to GVL were all carried out in a 10-mL Teflon-lined autoclave heated by an oil bath. In a general procedure, 1 mmol EL (144 mg), 72 mg of catalyst, and 5 mL of 2-propanol were added into the Teflon-lined reactor. The sealed reaction kettle was then put into the oil bath at a prefixed temperature, and the reaction time was accordingly recorded. After the reaction, the solid catalyst was removed by centrifugation, and the liquid mixture was passed through a filter membrane (0.22 μm) prior to GC and GC-MS analysis.

3.5. Product Analysis

Liquid products were identified using an Agilent 6890N GC-MS (Agilent, Santa Clara, CA, USA) with a 5973MS mass spectrometer. For the quantitative analysis of EL and GVL, an Agilent GC7890B equipped with a HP-5 19091J-413 column (30 m × 0.32 mm × 0.25 mm) and a flame ionization detector

(FID) was used. an internal standard method was adopted for the quantitative calculation based on standard curves ($R^2 > 0.99$) of EL and GVL, and naphthalene was used as the internal standard. Substrate conversion (X, %) and product yield (Y, %) were calculated using the following equations:

$$X\ (\%) = [1 - (\text{mole of substrate after reaction})/(\text{mole of initial substrate})] \times 100\%; \quad (1)$$

$$Y\ (\%) = (\text{mole of obtained product})/(\text{mole of initial substrate}) \times 100\%. \quad (2)$$

3.6. Catalyst Recycling

After each cycle of reactions, the catalyst was separated by centrifugation from the reaction mixture, successively washed with 10 mL of DMF, ethanol, and methanol, and then dried at 45 °C for 12 h. The resulting solid catalyst was directly used for the next run.

4. Conclusions

In summary, a stable Hf-containing acid–base bifunctional solid catalyst was prepared, and was determined to be highly efficient for the catalytic conversion of EL to GVL. A high GVL yield of 85% was obtained at 160 °C after 6 h, which was superior to the other tested catalysts. Acid and base sites were found to play a synergistic role in the hydrogenation step, while Brønsted acid species improved the adsorption of the substrate and the lactonization step, thus efficiently promoting the cascade reaction. In addition, the solid catalyst, PPOA–Hf-1.5, had good reusability, with five cycles of use without obvious activity decline.

Supplementary Materials: The following are available online at http://www.mdpi.com/2073-4344/8/7/264/s1, Table S1. Quantitative analysis data of chemical adsorption. Table S2. Percentage of atomic concentration on the catalyst surface by XPS. Figure S1. Pore diameter of HfO2 and recovered PPOA-Hf-1:1.5. Figure S2. STEM image and elemental mappings of PPOA-Hf-1:1.5. Figure S3. XPS spectra of in PPOA-Hf-x with different PPOA/Hf molar ratios.

Author Contributions: W.W., H.L., and S.Y. conceived and designed the experiments; W.W., Y.L., and W.Z. performed the experiments; W.W. and H.L. analyzed the data; and W.W., H.L., and S.Y. co-wrote the paper.

Funding: This study was financially supported by the National Natural Science Foundation of China (21576059 & 21666008), Fok Ying-Tong Education Foundation (161030), Guizhou Science & Technology Foundation ([2018]1037 & [2017]5788), and Key Technologies R&D Program of China (2014BAD23B01).

Conflicts of Interest: There are no conflicts to declare.

References

1. Xu, C.; Arancon, R.A.D.; Labidi, J.; Luque, R. Lignin depolymerisation strategies: Towards valuable chemicals and fuels. *Chem. Soc. Rev.* **2014**, *43*, 7485–7500. [CrossRef] [PubMed]
2. Li, H.; Saravanamurugan, S.; Yang, S.; Riisager, A. Direct transformation of carbohydrates to the biofuel 5-ethoxymethylfurfural by solid acid catalysts. *Green Chem.* **2016**, *18*, 726–734. [CrossRef]
3. Li, H.; Bhadury, P.S.; Riisager, A.; Yang, S. One-pot transformation of polysaccharides via multi-catalytic processes. *Catal. Sci. Technol.* **2014**, *4*, 4138–4168. [CrossRef]
4. Holm, M.S.; Saravanamurugan, S.; Taarning, E. Conversion of sugars to lactic acid derivatives using heterogeneous zeotype catalysts. *Science* **2010**, *328*, 602–605. [CrossRef] [PubMed]
5. Li, H.; Zhao, W.; Fang, Z. Hydrophobic Pd nanocatalysts for one-pot and high-yield production of liquid furanic biofuels at low temperatures. *Appl. Catal. B Environ.* **2017**, *215*, 18–27. [CrossRef]
6. Alonso, D.M.; Wettstein, S.G.; Dumesic, J.A. Bimetallic catalysts for upgrading of biomass to fuels and chemicals. *Chem. Soc. Rev.* **2012**, *41*, 8075–8098. [CrossRef] [PubMed]
7. Corma, A.; Iborra, S.; Velty, A. Chemical routes for the transformation of biomass into chemicals. *Chem. Rev.* **2007**, *107*, 2411–2502. [CrossRef] [PubMed]
8. Liguori, F.; Moreno-Marrodan, C.; Barbaro, P. Environmentally friendly synthesis of γ-valerolactone by direct catalytic conversion of renewable rources. *ACS Catal.* **2015**, *5*, 1882–1894. [CrossRef]

9. Li, H.; Yang, S.; Riisager, A.; Pandey, A.; Sangwan, R.S.; Saravanamurugan, S.; Luque, R. Zeolite and zeotype-catalysed transformations of biofuranic compounds. *Green Chem.* **2016**, *18*, 5701–5735. [CrossRef]
10. Zhang, Z. Synthesis of γ-valerolactone from carbohydrates and its applications. *ChemSusChem* **2016**, *9*, 156–171. [CrossRef] [PubMed]
11. Qi, X.; Guo, H.; Li, L.Y.; Smith, R.L., Jr. Acid-catalyzed dehydration of fructose into 5-hydroxymethylfurfural by cellulose-derived amorphous carbon. *ChemSusChem* **2012**, *5*, 2411–2502. [CrossRef] [PubMed]
12. Zhou, P.; Zhang, Z. One-pot catalytic conversion of carbohydrates into furfural and 5-hydroxymethylfurfural. *Catal. Sci. Technol.* **2016**, *6*, 3694–3712. [CrossRef]
13. Guo, H.; Duereh, A.; Hiraga, Y.; Aida, T.M.; Qi, X.; Smith, R.L., Jr. Perfect recycle and mechanistic role of hydrogen sulfate ionic liquids as additive in ethanol for efficient conversion of carbohydrates into 5-ethoxymethylfurfural. *Chem. Eng. J.* **2017**, *323*, 287–294. [CrossRef]
14. Guo, H.; Qi, X.; Hiraga, Y.; Aida, T.M.; Smith, R.L., Jr. Efficient conversion of fructose into 5-ethoxymethylfurfural with hydrogen sulfate ionic liquids as co-solvent and catalyst. *Chem. Eng. J.* **2017**, *314*, 508–514. [CrossRef]
15. Saravanamurugan, S.; Van Buu, O.N.; Riisager, A. Conversion of mono- and disaccharides to ethyl levulinate and ethyl pyranoside with sulfonic acid-functionalized ionic liquids. *ChemSusChem* **2011**, *4*, 723–726. [CrossRef] [PubMed]
16. Saravanamurugan, S.; Riisager, A. Solid acid catalysed formation of ethyl levulinate and ethyl glucopyranoside from mono- and disaccharides. *Catal. Commun.* **2012**, *17*, 71–75. [CrossRef]
17. Isikgor, F.H.; Becer, C.R. Lignocellulosic biomass: A sustainable platform for the production of bio-based chemicals and polymers. *Polym. Chem.* **2015**, *6*, 4497–4559. [CrossRef]
18. Saravanamurugan, S.; Riisager, A. Zeolite catalyzed transformation of carbohydrates to alkyl levulinates. *ChemCatChem* **2013**, *5*, 1754–1757. [CrossRef]
19. Gilkey, M.J.; Xu, B. Heterogeneous catalytic transfer hydrogenation as an effective pathway in biomass upgrading. *ACS Catal.* **2016**, *6*, 1420–1436. [CrossRef]
20. Li, J.; Liu, J.; Zhou, H.; Fu, Y. Catalytic transfer hydrogenation of furfural to furfuryl alcohol over nitrogen-doped carbon-supported iron catalysts. *ChemSusChem* **2016**, *9*, 1339–1347. [CrossRef] [PubMed]
21. Wang, D.; Astruc, D. The golden age of transfer hydrogenation. *Chem. Rev.* **2015**, *115*, 6621–6686. [CrossRef] [PubMed]
22. Grasemann, M.; Laurenczy, G. Formic acid as a hydrogen source–recent developments and future trends. *Energy Environ. Sci.* **2012**, *5*, 8171–8181. [CrossRef]
23. Bigler, R.; Huber, R.; Stöckli, M.; Mezzetti, A. Iron(II)/$(NH)_2P_2$ macrocycles: Modular, highly enantioselective transfer hydrogenation catalysts. *ACS Catal.* **2016**, *6*, 6455–6464. [CrossRef]
24. Li, H.; He, J.; Riisager, A.; Saravanamurugan, S.; Song, B.; Yang, S. Acid-base bifunctional zirconium *N*-alkyltriphosphate nanohybrid for hydrogen transfer of biomass-derived carboxides. *ACS Catal.* **2016**, *6*, 7722–7727. [CrossRef]
25. Wang, J.; Okumura, K.; Jaenicke, S.; Chuah, G.K. Post-synthesized zirconium-containing beta zeolite in Meerwein-Ponndorf-Verley reduction: Pros and cons. *Appl. Catal. A* **2015**, *493*, 112–120. [CrossRef]
26. Assary, R.S.; Curtiss, L.A.; Dumesic, J.A. Exploring Meerwein-Ponndorf-Verley reduction chemistry for biomass catalysis using a first-principles approach. *ACS Catal.* **2013**, *3*, 2694–2704. [CrossRef]
27. Chia, M.; Dumesic, J.A. Liquid-phase catalytic transfer hydrogenation and cyclization of levulinic acid and its esters to γ-valerolactone over metal oxide catalysts. *Chem. Commun.* **2011**, *47*, 12233–12235. [CrossRef] [PubMed]
28. Tang, X.; Hu, L.; Sun, Y.; Zhao, G.; Hao, W.; Lin, L. Conversion of biomass-derived ethyl levulinate into γ-valerolactone via hydrogen transfer from supercritical ethanol over a ZrO_2 catalyst. *RSC Adv.* **2013**, *3*, 10277–10284. [CrossRef]
29. Tang, X.; Chen, H.; Hu, L.; Hao, W.; Sun, Y.; Zeng, X.; Lin, L.; Liu, S. Conversion of biomass to γ-valerolactone by catalytic transfer hydrogenation of ethyl levulinate over metal hydroxides. *Appl. Catal. B Environ.* **2014**, *147*, 827–834. [CrossRef]
30. Li, H.; Fang, Z.; Yang, S. Direct conversion of sugars and ethyl levulinate into γ-valerolactone with superparamagnetic acid-base bifunctional $ZrFeO_x$ nanocatalysts. *ACS Sustain. Chem. Eng.* **2016**, *4*, 236–246. [CrossRef]
31. He, J.; Li, H.; Lu, Y.; Liu, Y.; Wu, Z.; Hu, D.; Yang, S. Cascade catalytic transfer hydrogenation-cyclization of ethyl levulinate to γ-valerolactone with Al-Zr mixed oxides. *Appl. Catal. A Gen.* **2016**, *510*, 11–19. [CrossRef]

32. He, J.; Li, H.; Liu, Y.; Zhao, W.; Yang, T.; Xue, W.; Yang, S. Catalytic transfer hydrogenation of ethyl levulinate into γ-valerolactone over mesoporous Zr/B mixed oxides. *J. Ind. Eng. Chem.* **2016**, *43*, 133–141. [CrossRef]
33. Tang, X.; Zeng, X.; Li, Z.; Li, W.; Jiang, Y.; Hu, L.; Liu, S.; Sun, Y.; Lin, L. In situ generated catalyst system to convert biomass-derived levulinic acid to γ-valerolactone. *ChemCatChem* **2015**, *7*, 1372–1379. [CrossRef]
34. Kuwahara, Y.; Kaburagi, W.; Osada, Y.; Fujitani, T.; Yamashita, H. Catalytic transfer hydrogenation of biomass-derived levulinic acid and its esters to γ-valerolactone over ZrO_2 catalyst supported on SBA-15 silica. *Catal. Today* **2017**, *281*, 418–428. [CrossRef]
35. de los Reyes, M.; Majewski, P.J.; Scales, N.; Luca, V. Hydrolytic stability of mesoporous zirconium titanate frameworks containing coordinating organic functionalities. *ACS Appl. Mater. Interfaces* **2013**, *5*, 4120–4128. [CrossRef] [PubMed]
36. Li, H.; Yang, T.; Fang, Z. Biomass-derived mesoporous Hf-containing hybrid for efficient Meerwein-Ponndorf-Verley reduction at low temperatures. *Appl. Catal. B Environ.* **2018**, *227*, 79–89. [CrossRef]
37. Gelman, F.; Blum, J.; Avnir, D. Acids and bases in one pot while avoiding their mutual destruction. *Angew. Chem. Int. Ed.* **2001**, *40*, 3647–3649. [CrossRef]
38. Yang, Y.; Liu, X.; Li, X.; Zhao, J.; Bai, S.; Liu, J.; Yang, Q. A yolk-shell nanoreactor with a basic core and an acidic shell for cascade reactions. *Angew. Chem.* **2012**, *124*, 9298–9302. [CrossRef]
39. Margelefsky, E.L.; Zeidan, R.K.; Davis, M.E. Cooperative catalysis by silica-supported organic functional groups. *Chem. Soc. Rev.* **2008**, *37*, 1118–1126. [CrossRef] [PubMed]
40. Li, H.; Fang, Z.; Smith, R.L., Jr.; Yang, S. Efficient valorization of biomass to biofuels with bifunctional solid catalytic materials. *Prog. Energy Combust. Sci.* **2016**, *55*, 98–194. [CrossRef]
41. Veliscek-Carolan, J.; Hanley, T.L.; Luca, V. Zirconium organophosphonates as high capacity, selective lanthanide sorbents. *Sep. Purif. Technol.* **2014**, *129*, 150–158. [CrossRef]
42. Zhu, Y.; Ma, T.; Liu, Y.; Ren, T.; Yuan, Z. Metal phosphonate hybrid materials: From densely layered to hierarchically nanoporous structures. *Inorg. Chem. Front.* **2014**, *1*, 360–383. [CrossRef]
43. Ma, T.; Yuan, Z. Metal phosphonate hybrid mesostructures: Environmentally friendly multifunctional materials for clean energy and other applications. *ChemSusChem* **2011**, *4*, 1407–1419. [CrossRef] [PubMed]
44. Bhanja, P.; Bhaumik, A. Organic-inorganic hybrid metal phosphonates as recyclable heterogeneous catalysts. *ChemCatChem* **2016**, *8*, 1607–1616. [CrossRef]
45. Silbernagel, R.; Martin, C.H.; Clearfield, A. Zirconium (IV) phosphonate-phosphates as efficient ion-exchange materials. *Inorg. Chem.* **2016**, *55*, 1651–1656. [CrossRef] [PubMed]
46. Li, H.; Liu, X.; Yang, T.; Zhao, W.; Saravanamurugan, S.; Yang, S. Porous zirconium-furandicarboxylate microspheres for efficient redox conversion of biofuranics. *ChemSusChem* **2017**, *10*, 1761–1770. [CrossRef] [PubMed]
47. Tang, B.; Dai, W.; Sun, X.; Wu, G.; Guan, N.; Hunger, M.; Li, L. Mesoporous Zr-Beta zeolites prepared by a post-synthetic strategy as a robust Lewis acid catalyst for the ring-opening aminolysis of epoxides. *Green Chem.* **2015**, *17*, 1744–1755. [CrossRef]
48. Song, J.; Zhou, B.; Zhou, H.; Wu, L.; Meng, Q.; Liu, Z.; Han, B. Porous zirconium–phytic acid hybrid: A highly efficient catalyst for Meerwein–Ponndorf–Verley reductions. *Angew. Chem. Int. Ed.* **2015**, *54*, 9399–9403. [CrossRef] [PubMed]
49. Luo, H.; Consoli, D.F.; Gunther, W.R.; Román-Leshkov, Y. Investigation of the reaction kinetics of isolated Lewis acid sites in Beta zeolites for the Meerwein-Ponndorf-Verley reduction of methyl levulinate to γ-valerolactone. *J. Catal.* **2014**, *320*, 198–207. [CrossRef]
50. Assary, R.J.; Curtiss, L.A. Theoretical studies for the formation of γ-valero-lactone from levulinic acid and formic acid by homogeneous catalysis. *Chem. Phys. Lett.* **2012**, *541*, 21–26. [CrossRef]
51. Chalid, M.; Broekhuis, A.A.; Heeres, H.J. Experimental and kinetic modeling studies on the biphasic hydrogenation of levulinic acid to γ-valerolactone using a homogeneous water-soluble Ru-(TPPTS) catalyst. *J. Mol. Catal. A Chem.* **2011**, *341*, 14–21. [CrossRef]